

PAPER • OPEN ACCESS

Temperature dependency of silicon structures for magnetic field gradient sensing

To cite this article: Alexander Dabsch *et al* 2018 *J. Micromech. Microeng.* **28** 025002

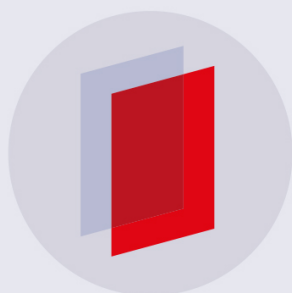
View the [article online](#) for updates and enhancements.

Related content

- [MEMS cantilever based magnetic field gradient sensor](#)
Alexander Dabsch, Christoph Rosenberg, Michael Stifter *et al.*
- [Multiaxial resonant MEMS force sensor](#)
Alexander Dabsch, Christoph Rosenberg, Patrick Klug *et al.*
- [Design and fabrication of a high performance resonant MEMS temperature sensor](#)
Talha Kose, Kivanc Azgin and Tayfun Akin

Recent citations

- [Multiaxial resonant MEMS force sensor](#)
Alexander Dabsch *et al*



IOP | ebooks™

Bringing you innovative digital publishing with leading voices to create your essential collection of books in STEM research.

Start exploring the collection - download the first chapter of every title for free.

Temperature dependency of silicon structures for magnetic field gradient sensing

Alexander Dabsch¹, Christoph Rosenberg¹, Michael Stifter^{1,2}
and Franz Keplinger¹

¹ Vienna University of Technology Institute of Sensor and Actuator Systems, Vienna,
Gusshausstraße 27-29, Austria

² Danube University Krems, Center for Integrated Sensor Systems, Wiener Neustadt, Viktor Kaplan
Straße 2, Austria

E-mail: alexander.dabsch@tuwien.ac.at

Received 4 April 2017, revised 30 June 2017

Accepted for publication 3 July 2017

Published 29 December 2017



CrossMark

Abstract

This work describes the temperature dependence of two sensors for magnetic field gradient sensors and demonstrates a structure to compensate for the drift of resonance frequency over a wide temperature range. The temperature effect of the sensing element is based on internal stresses induced by the thermal expansion of material, therefore FEM is used to determine the change of the eigenvalues of the sensing structure. The experimental setup utilizes a Helmholtz coil system to generate the magnetic field and to excite the MEMS structure with Lorentz forces. The MEMS structure is placed on a plate heated with resistors and cooled by a Peltier element to control the plate temperature. In the second part, we describe how one can exploit temperature sensitivity for temperature measurements and we show the opportunity to include the temperature effect to increase the sensitivity of single-crystal silicon made flux density gradient sensors.

Keywords: gradient sensor, temperature dependency, magnetic field, MEMS

(Some figures may appear in colour only in the online journal)

1. Introduction

Typical magnetic field gradient sensors based on MEMS technology [1] exhibit a temperature dependence of the resonant frequency that is mainly caused by the thermal expansion of the cantilever arms [2]. First, the sensors are built out of SOI wafers with a buried SiO₂-layer under the Si sensing structure. The thermal coefficient of expansion of these materials is four times lower than that of Si [3]. Second, the vibrating structure and carrier frame have different masses and therefore different heat capacities, leading to different temperatures in transient processes.

Due to these differences, temperature variations will expand or tighten the measuring structure faster than the

carrier frame. A mechanical stress is the consequence which alters the resonance frequency. The desired high quality factor of the structure causes a high error level in the amplitude due to temperature dependence [4]. In this work, a specific mechanical substructure is designed, fabricated and proposed to compensate for this temperature dependence (figure 1).

The sensors used within this paper are discussed in an earlier paper of our group regarding the sensitivity of the magnetic flux density gradient (see table 4) [5].

2. Theory

2.1. Extended Euler Bernoulli beam theory—Timoshenko beam theory

For the calculation of the temperature coefficient regarding the resonance frequency, the Euler Bernoulli beam theory must be extended with the bending and normal stresses.



Original content from this work may be used under the terms of the [Creative Commons Attribution 3.0 licence](https://creativecommons.org/licenses/by/3.0/). Any further distribution of this work must maintain attribution to the author(s) and the title of the work, journal citation and DOI.

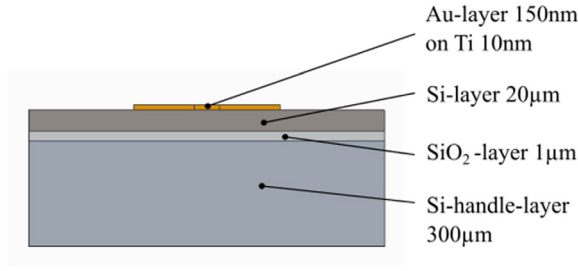


Figure 1. Structure of the MEMS sensor.

Only the first symmetric mode is investigated in our experiments. Hence, the Timoshenko theory can be simplified and applied to an oscillating solid-shell element for the H-shaped structure. The resonant frequency reads:

$$f = \frac{1}{2\widehat{L}} \frac{1}{\sqrt{\rho\nu}} \sqrt{P}, \quad (1)$$

where \widehat{L} is the length of the oscillating structure, ρ is the mass density, ν is the Poisson's ratio, and P is the force in longitudinal direction (prestress) [6].

For a long thin structure with small oscillating amplitude, a \sqrt{P} dependence is expected. The resultant force is generated by the geometry of the structure due to thermal expansion. In addition, with the effect of the prestress on the eigenvalues, the Timoshenko beam theory [7] is described by:

$$\frac{\partial^4 u_y}{\partial x^4} - \frac{P}{EI_z} \frac{\partial^2 u_y}{\partial x^2} + \frac{\rho A}{EI_z} \frac{\partial^2 u_y}{\partial t^2} = 0. \quad (2)$$

Due to the huge difference of the heat capacities of the free-standing structure and the carrier frame, the MEMS structure responds faster to temperature changes than the carrier frame. The occurring outer stresses can be approximately described as a function of the temperature difference of the measuring structure to the frame by:

$$\varepsilon_{\text{ges}} = \varepsilon_{\text{th}} + \varepsilon_{\text{m}}, \varepsilon_{\text{th}} = \alpha \cdot \Delta T, \varepsilon_{\text{m}} = \frac{\sigma}{E(T)}, \quad (3)$$

where ε_{ges} is the total strain, ε_{th} is the thermal strain, ε_{m} is the mechanical strain by stress, α is the thermal coefficient of expansion (TCE), σ is the tensile/compressive stress, and E is the Young's modulus [8].

For a small temperature range from 300 K to 350 K, the nonlinearity of the TCE of silicon is negligible. The occurring stress is

$$\sigma = -E(T) \cdot \alpha \cdot \Delta T. \quad (4)$$

The temperature coefficient from the Young's modulus of silicon for axial load is -60 ppm K^{-1} and for uniaxial load -75 ppm K^{-1} . The bending stiffness decreases with temperature [9].

For the theoretical consideration, we use the design of a torsional oscillator (figure 2).

Applying only antiparallel currents, we excite a pure torsional oscillation without any bending components (in the y -direction) due to the symmetric design. The oscillation mode with axial load P is described by:

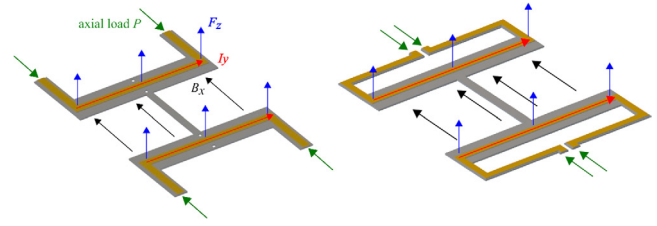


Figure 2. Layout of two structures with relevant Lorentz-forces (F_z) for the first symmetric modes with parallel current (I_y) direction (left: the double U-shaped structure, right: the omega-shaped structure). B_x is the magnetic flux density and P is the axial load by thermal expansion.

$$\left[GJ - \frac{PI_\alpha}{m} \right] \frac{\partial^2 \varphi}{\partial x^2} - I \frac{\partial^2 \varphi}{\partial t^2} = 0 \quad (5)$$

where G represents the shear modulus and J is the moment of inertia (in a good approximation, the moment of inertia of the bar), I is the polar mass moment of inertia per unit length, m represents the mass of the oscillator, and φ is the angular displacement of the bar [8].

- Applying (4) into design considerations, attention should be paid to some design details and boundary conditions: the plate in the middle of the oscillating system is short compared to the whole bar ($L_p < \widehat{L}$) and the torsional stiffness of the plate is much higher. The majority of the total torsion occurs in the bars.
- The neutral axis and the center of mass axis are congruent and are not subjected to any bending deformation.
- The static deflection of the bar caused by the gravitational force on the mass of the plate is neglected. The deflections act in the linear elastic regime and boundary effects in the connection between plate and bar are neglected.

Solving the eigenvalue problem delivers the eigenfrequency of the torsional mode (only the first antisymmetric mode with antiparallel current, depicted in figure 3 is calculated)

$$\omega_p = \frac{\pi}{\sqrt{\widehat{L}}} \sqrt{\left(\frac{GJ}{I} - \frac{P}{m} \right)}. \quad (6)$$

By setting P to zero the equation yields the eigenfrequency $\omega_0 = 4446 \text{ Hz}$ without any boundary load through thermal influences. The result of the simplified calculation is in good agreement with the experimental data (see chapter 4). The parameters used for the calculations are listed in table 1.

2.2. Influence of the temperature effect of the lead on the operating temperature

Due to strong frequency changes caused by small temperature variations, the heating power of the lead has to be taken into account. Therefore, the heat balance of the lead on the Si wafer under atmospheric influence is given by:

$$K(T) = P(T), \quad (7)$$

where $K(T)$ is the heat dissipation and $P(T)$ is the produced heat by the electrical current [10]. The heat dissipation to the

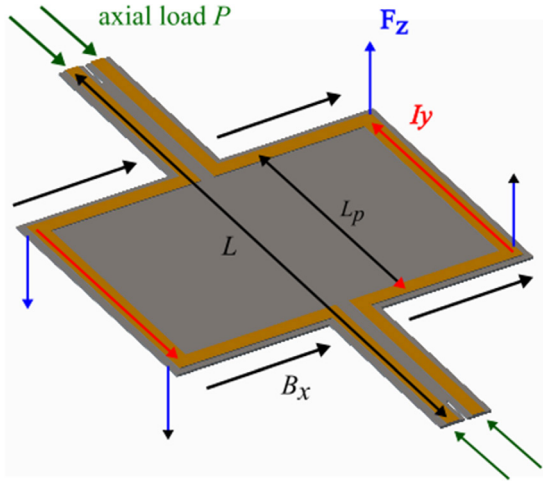


Figure 3. Design of the torsional oscillator with the forces (F_z) for the first torsional mode, with antiparallel currents (I_y), the whole length of the structure, plate and bars (L) and the length of the plate (L_p).

Table 1. Relevant parameters for the simulation of the silicon structure [8].

Symbol	Quantity	Value
G	Shear modulus	64.1 GPa
ν	Poisson ratio	0.28/0.2
\hat{L}	Free length	4 mm
J	Sec. moment of inertia	$2.66 \cdot 10^{-19} \text{ m}^4$
I	Moment of inertia per unit length	$5.32 \cdot 10^{-10} \text{ kg m}^2$
α	TCE	-60 ppm K^{-1} for axial load

surroundings can be split into three parts: heat conduction (\dot{Q}_{cond}), convection (\dot{Q}_{conv}) and thermal radiation (\dot{Q}_{rad}).

$$K(T) = \dot{Q}_{\text{cond}}(T) + \dot{Q}_{\text{conv}}(T) + \dot{Q}_{\text{rad}}(T) \quad (8)$$

$$\dot{Q}_{\text{cond}}(T) = \lambda \frac{T_2 - T_1}{h} A_s$$

$$\dot{Q}_{\text{conv}}(T) = \alpha(T) A_s (T_2 - T_e) \quad (9)$$

$$\dot{Q}_{\text{rad}}(T) = \varepsilon \sigma A_s (T_2^4 - T_e^4), \quad (10)$$

where T_2 is the temperature of the lead, T_1 is the temperature of the Si wafer, h is the thickness of the lead path, A_s is the contact surface of the lead with Si structure, and T_e is the ambient temperature.

To calibrate the sensor, the temperature of the sensor frame (silicon wafer) must be known. The energy balance is:

$$P(T) = \hat{U}_{\text{eff}} I \quad (11)$$

$$\hat{U}_{\text{eff}} I = \lambda \frac{T_2 - T_1}{h} A_s + \alpha(T) A_s (T_2 - T_e) + \varepsilon \sigma A_s (T_2^4 - T_e^4) \quad (12)$$

$$\begin{aligned} \xrightarrow{\text{convert}} T_1 &= \frac{h}{\lambda} \left[\alpha(T) (T_2 - T_e) + \varepsilon \sigma (T_2^4 - T_e^4) + \frac{\hat{U}_{\text{eff}} I}{A_s} \right] \\ &= 31.209 \text{ }^\circ\text{C}. \end{aligned} \quad (13)$$

To calculate T_2 , the resistance of the lead with stable power supply was recorded:

$$R_1 = \frac{L_{\text{LB}}}{A_q} \rho_{20} (1 + \alpha_R \Delta T_1) \text{ and} \quad (14)$$

$$R_2 = \frac{L_{\text{LB}}}{A_q} \rho_{20} (1 + \alpha_R \Delta T_2), \quad (15)$$

where R_1 is the electrical resistance of the lead at room temperature, R_2 is the electrical resistance of the lead after 15 min of the temperature change, L_{LB} is the length of the lead, and A_q is the cross section of the lead. With the measurement results T_2 becomes:

$$T_2 = \Delta T_2 - T_R = 31.211 \text{ }^\circ\text{C}. \quad (16)$$

The dominating term is \dot{Q}_{cond} , which is 70 times larger than \dot{Q}_{conv} and 1600 times larger than \dot{Q}_{rad} . $\dot{Q}_{\text{cond}}(T) = 2.33 \text{ mW}$, $\dot{Q}_{\text{conv}}(T) = 0.033 \text{ mW}$, $\dot{Q}_{\text{rad}}(T) = 0.0014 \text{ mW}$.

Therefore, for measurements at room temperature and considering the actual geometry, $\dot{Q}_{\text{conv}}(T)$ and $\dot{Q}_{\text{rad}}(T)$ can be neglected. The parameters used for the calculations are listed in table 2.

2.3. Material specifications

The applied material is [100] silicon featuring an anisotropic Young's modulus of 170 GPa in 1 1 1 directions and reduced values down to 130 GPa for all other directions [9].

Via the lithography process, thin gold leads with a thickness of 150 nm are deposited on the silicon structure. These leads are insignificant for the thermal tensile or compressive stress due to the Young's modulus of 78 GPa being 2.2 times higher than that of silicon and the lead being 100 times thinner than the silicon structure.

During Au evaporation, mechanical stress is introduced in the metal layer and consequently within the Si-structure. Afterwards, this pre-stress is minimised by a thermal treatment at 90 °C for 1 h.

Between the sensor and the Pt100 element (see figures 6 and 7), a two-component conductive silver epoxy is used as an intermediate layer.

3. Simulations

As a first step, the temperature dependency is simulated with the FEM-software COMSOL® Multiphysics 5.2.

Different designs are tested with FEM simulation. Figures 4 and 5 depict the temperature dependence of the resonant frequency of the first six modes. The reference temperature is set to 300 K [1].

For modelling, we assume that there is no thermal expansion of the frame surrounding the oscillating structure. A temperature difference between frame and silicon based structure is set. For this reason, the supporting points of the structure are fixed in the axial direction. Avoiding torsion of the gradient structures (plate) the suspension bars are not generally fixed in the radial direction.

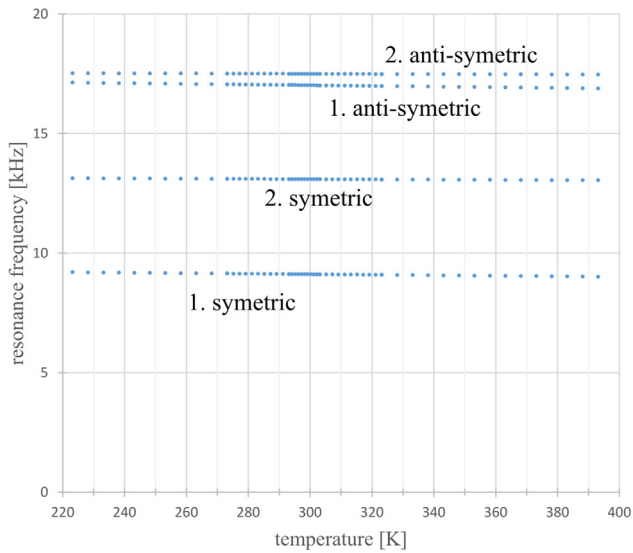


Figure 4. Simulated temperature dependence of the resonance frequencies of the first six modes of the omega-shaped design.

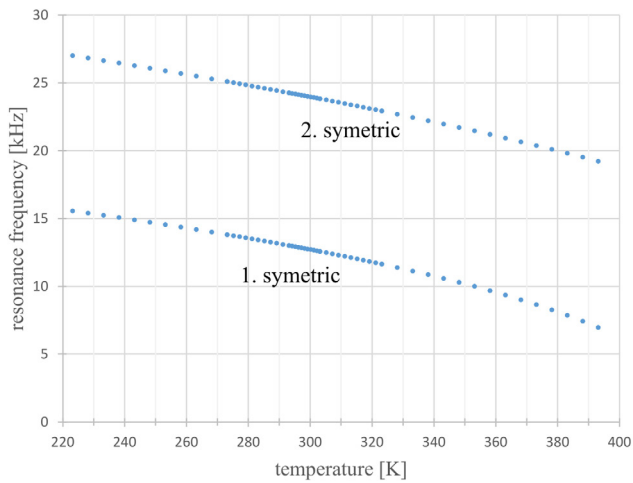


Figure 5. Simulated temperature dependence of the resonance frequencies of the first six modes for the double U-shaped design.

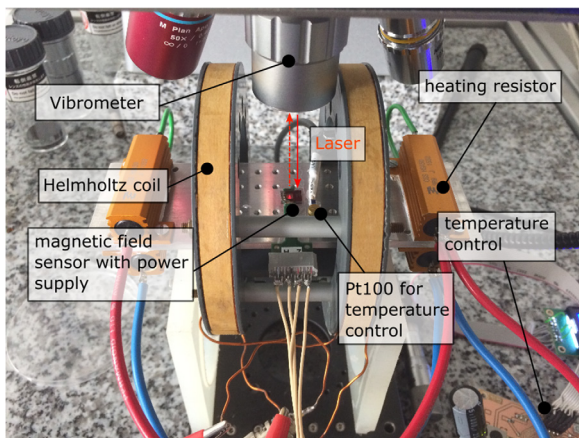


Figure 6. Measurement setup with Helmholtz coils, heating plate and readout with the vibrometer.

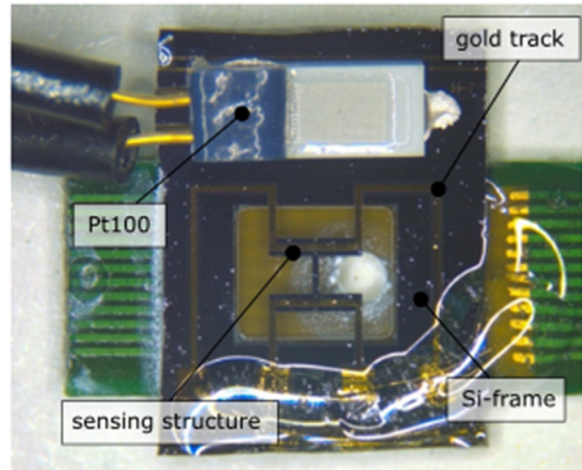


Figure 7. Double U-shaped design with a Pt100 fixed with a silver thermal adhesive.

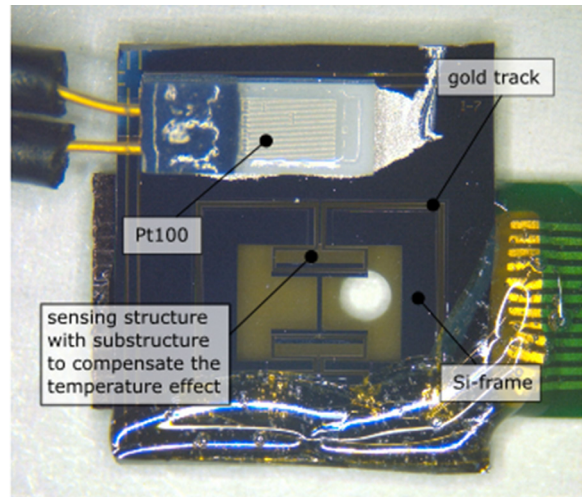


Figure 8. Omega-shaped design.

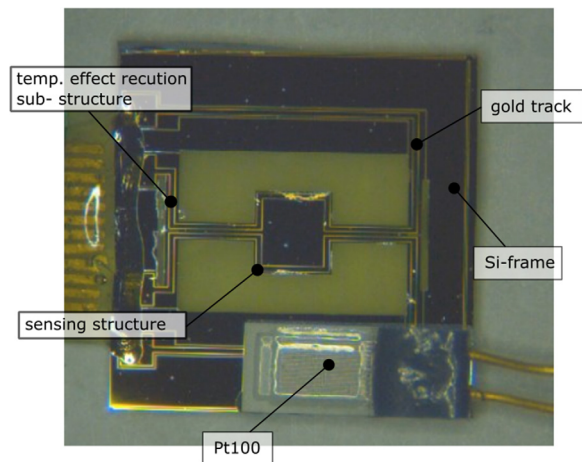


Figure 9. Torsional oscillator design.

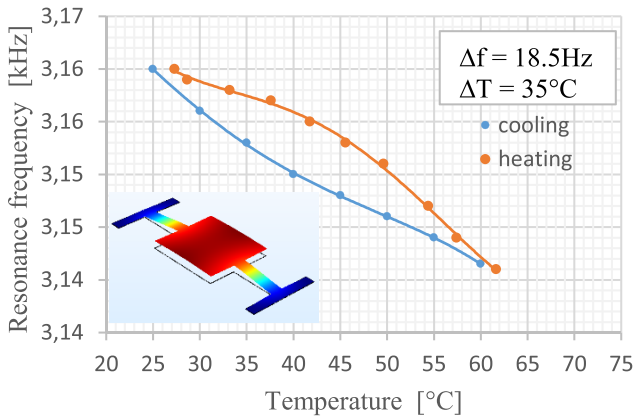


Figure 10. Measured temperature induced change of the resonant frequency of the first symmetric mode.

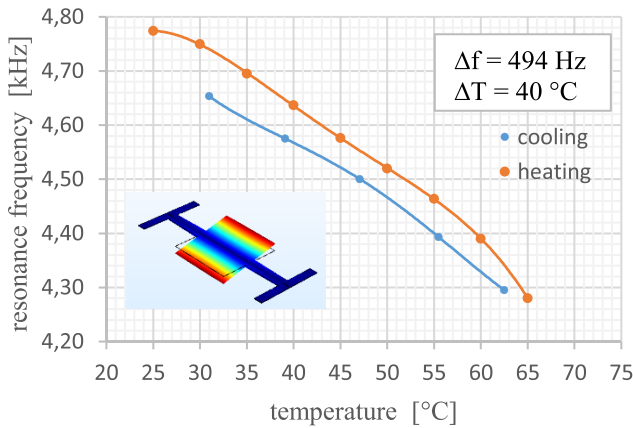


Figure 11. Measured change of the resonant frequency of the first antisymmetric (torsional) mode from the torsional bending structure in dependence of the temperature.

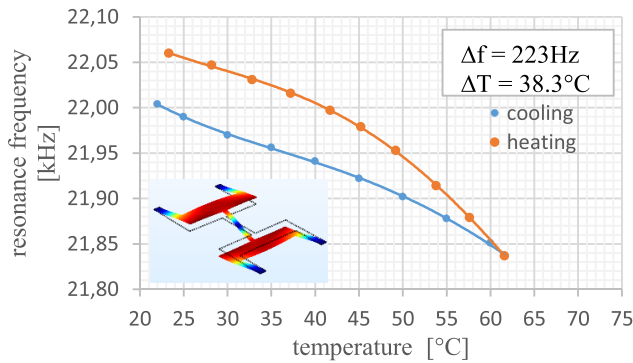


Figure 12. Measured change of the resonant frequency of the second symmetric mode from the double U-shaped structure in dependence of the temperature.

Comparing figures 4 and 5 illustrates that the omega-shaped structure has a lower adjustment of the resonant frequency. This is due to the smaller stiffness in the x -direction, caused by the meander sub structure (figure 2).

4. Measurements

The measurement setup comprises a set of Helmholtz coils where the sensor is fixed in the center on a plate that can be heated up. The leads on the structure are connected to

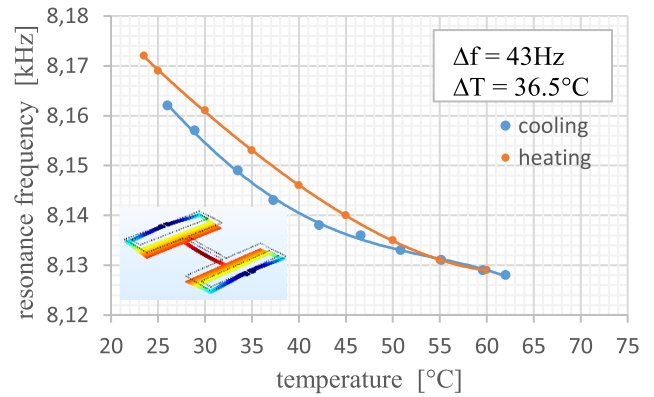


Figure 13. Measured change of the resonant frequency of the first symmetric mode from the omega-shaped structure in dependence of the temperature.

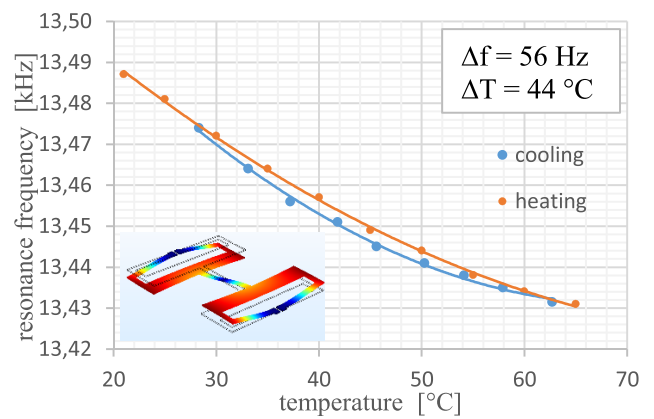


Figure 14. Measured change of the resonant frequency of the second symmetric mode from the omega-shaped structure in dependence of the temperature.

Table 2. Relevant parameters for the calculation of the heat balance.

Symbol	Quantity	Value
λ_s	Thermal conductivity coefficient	$117 \text{ W m}^{-1} \text{ K}^{-1}$
$\alpha(T)$	Convection coefficient for free convection	$6 \text{ W m}^{-2} \text{ K}$
ϵ_{Au}	Emission coefficient	0.04
σ	Stefan-Boltzmann constant	$5.6 \cdot 10^{-8} \text{ W (m}^2 \text{ K}^4)^{-1}$
ρ_{20}	Specific resistance of gold at room temperature	$2.2 \cdot 10^{-2} \Omega \text{ mm}^2 \text{ m}^{-1}$
α_R	Temperature coefficient of specific resistance	$3.7 \cdot 10^{-3} \text{ 1/K}$

a waveform generator that produces a periodic chirp in the range of 500 Hz around the resonant frequency of the selected sensor. The deflections are recorded with a Micro System Analyzer (MSA 400, Polytec).

The heat control plate is made from aluminum equipped with a PT100 element and four heating resistors driven by a PWM controller. To avoid any interferences with the magnetic field of the two Helmholtz coils, the heat resistors are placed outside of the coils. For good heat transfer and low distortions of the magnetic field, aluminum (with its paramagnetic

Table 3. Operating parameters.

Symbol	Quantity	Value
U_{ss}	Stimulation voltage	1 V
I_s	Parallel current mode	2.3 mA
I_H	Current Helmholtz coils	1 A
B	Magnetic field	5.4 mT

Table 4. Used structure types with sensitivities for magnetic field gradient and temperature sensitivities.

Structure	Sensitivity (mT mm ⁻¹)	Temp. sensitivity (Hz K ⁻¹)
U-shaped (second symmetric mode)	0.09	5.8
Omega-shaped (second symmetric mode)	0.1	1.3
Torsional structure (first anti-symmetric mode)	^a	12.4
Torsional structure (first symmetric mode)	0.24	0.53

^a It is not possible to measure a field gradient with the torsional bending structure at the anti-symmetric modes.

properties) is used. In the middle of the plate, directly on the surface, the PT100 element is placed, measuring the actual temperature of the plate. The controller allows the adjustment of the temperature in a range from room temperature up to 100 °C.

To measure the temperature of the sensor, more precisely the Si-frame, another Pt100 element is mounted directly on the Si structure (see figures 7 and 8). The limited heat transfer between the aluminum plate and the sensor will cause a slight temperature difference. The result of the sensor Pt100 element is the actual temperature for the device (reference temperature for the subsequent measurements).

The measurements are performed with the highest possible continuous load of the Helmholtz coil, see table 3 for operating parameters. With lower flux densities, no significant change in the temperature dependency has been determined.

5. Conclusion and outlook

The drift of the resonance frequency during heating and cooling is measured versus the temperature (recorded with a second Pt100 element directly on the surface of the Si structure) for three different sensor designs. Except for the torsional mode from the torsional bending structure (figures 10 and 11), the depicted results are in good agreement with the simulations (figures 4 and 5) and show a hysteresis between heating and cooling. This effect is caused, first by the positioning of the heat plate under the sensor and the single-sided heat supply during the heating process. Second, during the cooling process, heat dissipation only occurs on the upper surface of the sensor where the Pt100 element is fixed. Third, by the high self-cooling rate (approximately 1 °C per second) without heat supply. To avoid influences from the excitation current, it is switched off during the heating and cooling processes.

The measurements reveal the differences between the U-shaped design and the omega-shaped design (figures 12–14) with the temperature effect –compensating substructures (see table 4). Using two sensors with the same sensitivity for the magnetic flux density gradient, the temperature effect decreases from 5.8 Hz K⁻¹ (U-shaped) to 1.3 Hz K⁻¹ (omega-shaped). In particular, this effect occurs in the case of symmetric modes due to buckling. However, no significant differences between both structure types are seen for antisymmetric modes.

The torsional bending structure has a temperature effect of 0.5 Hz K⁻¹ using the first symmetric mode (comparable with a both side fixed beam) caused by the additional mass in the center of the beam and the temperature-effect-compensation sub-structure (see figure 9), but 12.4 Hz K⁻¹ using the first torsional mode (which is used for the magnetic flux density gradient measurement).

Subsequently to this basic characterization, the research team aim at another set of different sensors with capacitive readout as magnetic field gradient sensor on the one hand and as high sensitive temperature sensor on the other hand. The structure is very sensitive to changes to the force on the supporting points. The team will use this effect to fabricate a multiaxial force sensor with high sensitivity.

Acknowledgments

The authors acknowledge the TU Wien University Library for financial support through its Open Access Funding Program.

References

- [1] Stifter M 2012 *Lorentz Force Actuated Resonant MEMS Magnetometer with Capacitive Read-Out* (Vienna: University of Technology)
- [2] Sandberg R 2005 Temperature and pressure dependence of resonance in multi-layer microcantilevers *J. Micromech. Microeng.* **15** 1454–8
- [3] Sinha A K 1978 Thermal stresses and cracking resistance of dielectric films (SiN, Si₃N₄ and SiO₂) on Si substrates *J. Appl. Phys.* **49** 2423
- [4] Acevedo-Mijangos J, Soler-Balcázar C, Vazquez-Leal H, Martínez-Castillo J and Herrera-May A L 2013 Design and modeling of a novel microsensor to detect magnetic fields in two orthogonal directions *Microsyst. Technol.* **19** 1897
- [5] Dabsch A 2017 MEMS cantilever based magnetic field gradient sensor *J. Micromech. Microeng.* **27**
- [6] Rohrbach C 1989 *Handbuch für experimentelle Spannungsanalyse* (Berlin: Springer) p 590
- [7] Yang J 2010 *Nonlinear Free Vibration of Single-Walled Carbon Nanotubes Using Nonlocal Timoshenko Beam Theory* (New York: Elsevier)
- [8] Banerjee J R 1994 Coupled bending-torsional dynamic stiffness matrix of an axially loaded Timoshenko beam element *Int. J. Solids Struct.* **31** 749–62
- [9] Hopcroft M A, Nix W D and Kenny T W 2010 What is the Young's modulus of silicon *J. Microelectromech. Syst.* **19** 229–38
- [10] Baehr H D and Stephan K 2004 *Wärme- und Stoffübergang* 4th edn (Berlin: Springer) ch 5